

# Thermalisation as Diffusion in Hilbert Space.

A.V. Lunkin<sup>1\*</sup>

<sup>1</sup> Nanocenter CENN, Jamova 39, Ljubljana, SI-1000, Slovenia

\* Aleksey.Lunkin@nanocenter.si

March 13, 2026

## Abstract

We develop a microscopic theory of thermalisation for a thermometer coupled to a many-body bath beyond standard Markovian and Fermi-golden-rule assumptions. By modeling interaction matrix elements in the non-interacting basis as independent random variables, we derive a diffusion-propagator expression for the reduced dynamics and show that relaxation is controlled by the distribution of interaction-induced level broadenings. The theory predicts a thermalisation timescale set by the inverse typical broadening and yields a non-Markovian generalization of global balance. Exact-diagonalization tests for heavy-tailed Lévy couplings, an all-to-all transverse-field Ising model, and the one-dimensional Imbrie model show good agreement with these predictions.

---

## Contents

<b>1</b>	<b>Introduction</b>	<b>2</b>
<b>2</b>	<b>Diffusion propagator.</b>	<b>2</b>
<b>3</b>	<b>Cavity equation.</b>	<b>4</b>
<b>4</b>	<b>Emergence of diffusion</b>	<b>5</b>
<b>5</b>	<b>Single spin thermalisation</b>	<b>7</b>
	5.1 Lévy model.	7
	5.2 TFIM	8
	5.3 Imbrie model.	9
<b>6</b>	<b>Discussion and conclusion</b>	<b>10</b>
	<b>References</b>	<b>11</b>

---

## 1 Introduction

Understanding thermalisation in closed quantum systems remains a central problem in modern physics. A common starting point is the eigenstate thermalisation hypothesis (ETH) [1, 2, 3], which models matrix elements of local observables in the many-body eigenbasis as random variables whose variance varies smoothly with energy. For reviews, see Refs. [4, 5]. ETH explains why long-time local observables approach thermal values for states with narrow energy support. However, ETH alone does not provide controlled predictions for thermalisation times. It is also difficult to extract robust distribution parameters from finite-size numerics [6, 7]. The problem is especially severe in disordered systems, where matrix-element statistics are often broad and strongly non-Gaussian [8, 9, 10].

Reduced dynamics of a subsystem coupled to a bath is often described by master (Lindblad) equations. This usually assumes Markovian dynamics with transition rates estimated by Fermi's golden rule (FGR). In strongly disordered interacting systems, both assumptions can fail because localization effects in Hilbert space become important [11, 12, 13, 8]. This phenomenon is known as many-body localization (MBL) [14, 15]. Even outside the localized phase, broad distributions of relaxation rates are expected [13, 8, 16]. As a result, the quantitative link between Hilbert-space transition rates and experimentally relevant real-space relaxation remains incomplete.

Recent quantum-processor experiments highlight this gap: real-space dynamics can appear frozen while relaxation in Hilbert space continues and follows broad, often power-law statistics [17]. This behavior is naturally connected to spin-glass phenomenology [18, 19, 20, 21]. It also raises broader questions about slow modes, finite-size effects, and the delocalization crossover [22, 23, 24, 25, 26, 27, 17]. These developments motivate a dynamical framework that remains valid beyond the standard Markovian and FGR regimes.

In this work, we study a composite system consisting of a small thermometer and a large bath. We model interaction matrix elements in the non-interacting basis as independent random variables, without assuming finite variance. First, we derive a relation between reduced thermometer dynamics and the distribution of bath-state level broadenings. Second, we show that this relation yields thermalisation of the thermometer on a timescale set by the inverse typical broadening. We also derive a non-Markovian generalization of the global balance equation.

The structure of this work is as follows. In Sec. 2, we introduce the setup and the main quantities. In Sec. 3, we derive the cavity equation, and in Sec. 4 we generalize the approach to describe the statistics of off-diagonal Green-function matrix elements. In Sec. 5, we test our predictions numerically. Finally, in Sec. 6 we discuss the main implications and limitations of our results.

## 2 Diffusion propagator.

We consider a system described by the Hamiltonian

$$\hat{H} = \hat{H}_T + \hat{H}_B + \hat{V}_{int}, \quad (1)$$

where  $\hat{H}_T$  and  $\hat{H}_B$  denote the Hamiltonians of the thermometer and the bath, respectively, and  $\hat{V}_{int}$  describes their interaction. We use Latin and Greek indices to label eigenstates of the

bath and the thermometer, respectively. Eigenstates of the non-interacting system ( $\hat{V}_{int} = 0$ ) are labeled by bold Latin indices  $\mathbf{j}$ , or by pairs  $(\alpha, j)$ .

The joint probability that the thermometer is initially in state  $\beta$  and is in state  $\alpha$  at time  $t > 0$  is

$$p_{\alpha\beta}(t) = \text{Tr} \left[ \hat{P}_\alpha(t) \hat{P}_\beta \hat{\rho} \right]. \quad (2)$$

Here  $\hat{P}_\alpha \equiv |\alpha\rangle\langle\alpha| \otimes \hat{1}$  is the projector onto the thermometer state  $|\alpha\rangle$ , and  $\hat{\rho}$  denotes the density matrix of the full system.

We focus on the dynamics of diagonal elements of the reduced density matrix of the thermometer, assuming that the interaction does not renormalize the thermometer Hamiltonian. The dynamics of off-diagonal elements may play an important role in MBL and are left for future work.

We assume that the initial state has a well-defined energy; this is the only property of the density matrix relevant for our analysis. Under this assumption, the density matrix can be written as  $\hat{\rho} = f(\hat{H})$ . The function  $f$  is positive and satisfies the normalization condition  $\int d\epsilon N\nu(\epsilon)f(\epsilon) = 1$ , where  $\nu(\epsilon)$  is the normalized global density of states. We then introduce the distribution

$$P(\epsilon) \equiv \frac{f(\epsilon)}{N\nu(\epsilon)}. \quad (3)$$

The well-defined-energy condition means that this distribution is centered near a given energy and is narrower than the density of states. Then Eq. (2) can be rewritten as

$$p_{\alpha\beta}(t) = \int \frac{d\epsilon_+}{2\pi} \frac{d\epsilon_-}{2\pi} \text{Tr} \left[ \hat{P}_\alpha \hat{G}(\epsilon_+ + i0) \hat{P}_\beta \left( \hat{G}(\epsilon_- - i0) - \hat{G}(\epsilon_- + i0) \right) \right] \frac{P(\epsilon_-)}{N\nu(\epsilon_-)} e^{-i(\epsilon_+ - \epsilon_-)t}. \quad (4)$$

Here we introduced the Green function of the full system,  $\hat{G}(z) \equiv [z - \hat{H}]^{-1}$ . At sufficiently long times, the leading contribution comes from terms whose Green-function poles lie in different half-planes. We therefore rewrite the expression as

$$p_{\alpha\beta}(t) \approx \sum_{j,k} \int_{-\infty}^{\infty} \frac{d\epsilon}{2\pi} \int_{-i\infty}^{i\infty} \frac{d\mathcal{Z}}{2\pi i} \mathcal{D}_{(\alpha,j),(\beta,k)} \frac{P(\epsilon)}{\nu(\epsilon)} e^{\mathcal{Z}t}. \quad (5)$$

We define the propagator

$$D_{\mathbf{j}\mathbf{k}} = \text{Tr} \left[ \hat{P}_{\mathbf{j}} \hat{G} \left( \epsilon + i\frac{\mathcal{Z}}{2} \right) \hat{P}_{\mathbf{k}} \hat{G} \left( \epsilon - i\frac{\mathcal{Z}}{2} \right) \right], \quad \hat{P}_{(\alpha,j)} \equiv |\alpha\rangle\langle\alpha| \otimes |j\rangle\langle j|. \quad (6)$$

It is also convenient to introduce the propagator between thermometer states,

$$D_{\alpha,\beta} = \frac{1}{N} \sum_{j,k} \mathcal{D}_{(\alpha,j),(\beta,k)} = \text{Tr} \left[ \hat{P}_\alpha \hat{G} \left( \epsilon + i\frac{\mathcal{Z}}{2} \right) \hat{P}_\beta \hat{G} \left( \epsilon - i\frac{\mathcal{Z}}{2} \right) \right]. \quad (7)$$

We show that this expression leads to thermalisation regardless of  $P(\epsilon)$ , provided that the distribution is sufficiently narrow and the interaction produces nonzero level broadening.

The sum over bath states can be interpreted as an average. To evaluate it, we assume that the matrix elements of  $V_{int}$  are independent random variables. This assumption can be viewed as an application of ETH to the interaction operator  $V_{int}$ .

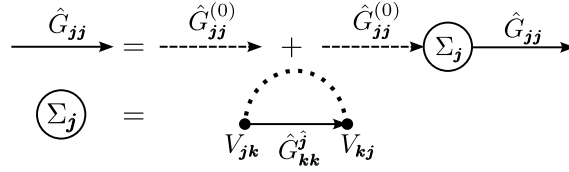


Figure 1: Diagrammatic representation of the cavity equation for the self-energy. Note the similarity to the standard non-crossing approximation, where the dashed line denotes a pairing according to Wick’s theorem. Here, the crossed line indicates that we only consider terms where two perturbation-matrix elements are complex conjugates.

The propagator in Eq. (6) involves products of Green-function matrix elements. We therefore start by analyzing diagonal matrix elements. This product of two Green functions is analytic in  $\varkappa$  in the right half-plane. For convenience, we first take  $\varkappa$  to be positive and real, and then perform analytic continuation.

### 3 Cavity equation.

We treat the interaction term  $V_{int}$  as a random matrix. This assumption simplifies the analysis in the large-matrix-size limit and leads to the cavity equation [19]. The cavity approximation is exact when the corresponding hopping Hamiltonian describes motion on a tree graph. It is also applicable to Hamiltonians represented by large dense matrices [28, 29]. The tree-graph analogy follows from a simple observation: for a random walk on the associated graph, the probability of forming a loop along a path of fixed length scales as  $1/N$ , where  $N$  is the dimension of the Hamiltonian. In our approach,  $N$  denotes the bath Hilbert-space dimension; this convention does not affect the estimate above. The cavity equation reads:

$$\left(\hat{G}_{jj}\right)^{-1} = \left(\hat{G}_{jj}^{(0)}\right)^{-1} - \Sigma_j, \quad \Sigma_j = \sum_{\mathbf{k}} |V_{j\mathbf{k}}|^2 \hat{G}_{\mathbf{k}\mathbf{k}}^j. \quad (8)$$

Here  $\hat{G}^{(0)}$  denotes the Green function of the non-interacting system, and  $\hat{G}_{\mathbf{k}\mathbf{k}}^j$  is the Green function of the Hamiltonian with the  $\mathbf{j}$ -th row and column removed. We use this notation for other cavity quantities below as well.

The structure of the cavity equation resembles a diagrammatic self-energy calculation (see Fig. 1). However, there is a qualitative difference between the two approaches. Standard crossed-diagram techniques assume a finite variance of matrix elements and therefore yield a self-averaging self-energy. In contrast, the cavity equation yields the full distribution of the self-energy, even when the second moment of matrix elements does not exist. If level broadening is self-averaging, it becomes independent of  $\varkappa$ , enabling the use of Fermi’s golden rule. For broadly distributed matrix elements, the self-energy distribution depends on  $\varkappa$  [29]. This may imply the absence of a local-in-time equation of motion for thermalisation, so the Markovian approximation becomes inapplicable. Nevertheless, as we show below, a thermal distribution can still emerge in this regime.

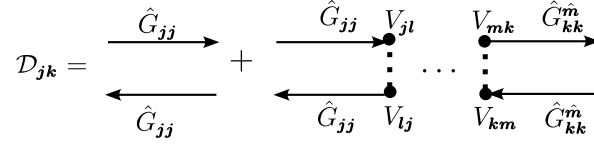


Figure 2: Diagrammatic representation of the leading contribution to the propagator from Eq. (6). The argument of the top Green function is  $\epsilon + i\mathcal{N}/2$ , whereas the argument of the bottom Green function is  $\epsilon - i\mathcal{N}/2$ .

## 4 Emergence of diffusion

We extend the diagrammatic analogy introduced above to evaluate the propagator in Eq. (6). As in the cavity-equation analysis, we begin with a Hamiltonian describing hopping on a tree. In this case, the off-diagonal Green-function matrix element between vertices  $\mathbf{j}_1$  and  $\mathbf{j}_n$  is

$$\hat{G}_{\mathbf{j}_1 \mathbf{j}_n} = \hat{G}_{\mathbf{j}_1 \mathbf{j}_1} \prod_{k=1}^{n-1} H_{\mathbf{j}_k \mathbf{j}_{k+1}} \hat{G}_{\mathbf{j}_{k+1} \mathbf{j}_{k+1}}^{\mathbf{j}_k}. \quad (9)$$

Here  $\mathbf{j}_1 \dots \mathbf{j}_k \dots \mathbf{j}_n$  denotes the tree path connecting vertices  $\mathbf{j}_1$  and  $\mathbf{j}_n$ .

We now switch to dense Hamiltonian matrices, where many paths connect a pair of vertices  $\mathbf{j}$  and  $\mathbf{k}$ . In the large- $N$  limit, each path can be treated as effectively non-crossing, so we apply the tree expression to each path and sum over them. The propagator in Eq. (6) contains a product of two Green functions, and we neglect interference terms in this product. This approximation is justified at times comparable to the inverse level spacing and leads to the following diffusive propagator:

$$\mathcal{D}_{\mathbf{j}\mathbf{k}} = \sum_{n=0} \sum_{\mathbf{j}_1 \dots \mathbf{j}_n | \mathbf{j}_1 = \mathbf{j}, \mathbf{j}_n = \mathbf{k}} \mathcal{B}_{\mathbf{j}_1} \prod_{k=1}^{n-1} |H_{\mathbf{j}_k \mathbf{j}_{k+1}}|^2 \mathcal{B}_{\mathbf{j}_{k+1}}^{\mathbf{j}_k}, \quad \mathcal{B}_{\mathbf{j}}^{\mathbf{i}} = \hat{G}_{\mathbf{j}\mathbf{j}}^{\mathbf{i}} \left( \epsilon + i\frac{\mathcal{N}}{2} \right) \hat{G}_{\mathbf{j}\mathbf{j}}^{\mathbf{i}} \left( \epsilon - i\frac{\mathcal{N}}{2} \right). \quad (10)$$

This approximation is the analogue of ladder-diagram summation in standard diagrammatic techniques (see Fig. 2). In standard crossed-diagram techniques, the sum of such ladder diagrams is referred to as a diffuson, and the corresponding approximation is known as the diffusion approximation; we adopt the same terminology here. When  $V_{\text{int}}$  is treated as a random matrix with independent elements, this approximation gives the leading contribution to the propagator in  $1/N$ .

We introduce the following notation for further analysis. First, we define the local density of states  $\nu$  and level broadening  $\Gamma$ :

$$\begin{aligned} \tilde{\nu}_{\mathbf{j}} &\equiv 2\pi\nu_{\mathbf{j}} \equiv i \left[ \hat{G}_{\mathbf{j}\mathbf{j}} \left( \epsilon + i\frac{\mathcal{N}}{2} \right) - \hat{G}_{\mathbf{j}\mathbf{j}} \left( \epsilon - i\frac{\mathcal{N}}{2} \right) \right], \\ \Gamma_{\mathbf{j}} &\equiv i \left[ \Sigma_{\mathbf{j}} \left( \epsilon + i\frac{\mathcal{N}}{2} \right) - \Sigma_{\mathbf{j}} \left( \epsilon - i\frac{\mathcal{N}}{2} \right) \right] = \sum_{\mathbf{k}} \Gamma_{\mathbf{j}\mathbf{k}}, \quad \Gamma_{\mathbf{j}\mathbf{k}} = |V_{\mathbf{j}\mathbf{k}}|^2 \tilde{\nu}_{\mathbf{k}}. \end{aligned} \quad (11)$$

We rewrite the product of two Green functions in the form

$$\mathcal{B}_{\mathbf{j}} = \frac{\tilde{\nu}_{\mathbf{j}}}{\mathcal{N} + \Gamma_{\mathbf{j}}}. \quad (12)$$

This correlator describes transitions in the full system. Each dashed line in Fig. 2 represents a transition between system states. Here we focus on transitions between thermometer states, so transition rates must be averaged over bath states. To evaluate the corresponding propagator, we sum over initial and final bath states according to Eq. (7).

In Eq. (10), the last factor  $\mathcal{B}_{j_n}^{\hat{j}_{n-1}}$  in each product is only weakly correlated with previous factors. Correlations with other  $\mathcal{B}$  terms are suppressed by  $1/N$ . Correlation with  $|H_{j_{n-1}, j_n}|^2$  is absent because this matrix element does not enter the definition of  $\mathcal{B}_{j_n}^{\hat{j}_{n-1}}$ . This allows us to replace this quantity by its average when evaluating the thermometer propagator in Eq. (7):

$$\mathcal{B}_\beta = \frac{1}{N} \sum_k \mathcal{B}_{(\beta,k)}^{\hat{j}_{n-1}} \approx \frac{1}{N} \sum_k \mathcal{B}_{(\beta,k)}. \quad (13)$$

However, to simplify the subsequent analysis, we need a slightly more involved replacement:

$$\mathcal{B}_{(\beta,k)}^{\hat{j}_{n-1}} \rightarrow \tilde{\nu}_{(\beta,k)}^{\hat{j}_{n-1}} \mathcal{B}_\beta / \tilde{\nu}_\beta, \quad \tilde{\nu}_\beta = \frac{1}{N} \sum_k \tilde{\nu}_{(\beta,k)}^{\hat{j}_{n-1}} \approx \frac{1}{N} \sum_k \tilde{\nu}_{(\beta,k)}. \quad (14)$$

The same argument justifies this replacement: the correlation between  $\tilde{\nu}_{(\beta,k)}^{\hat{j}_{n-1}}$  and all other terms is suppressed by  $1/N$ , so each factor can be replaced by its average, and vice versa.

We use this replacement to rewrite Eq. (7) as

$$\mathcal{D}_{\alpha\beta} = \left( \delta_{\alpha,\beta} + \frac{1}{N} \sum_j \sum_{n=1} \sum_{\mathbf{j}_1 \dots \mathbf{j}_n} \sum_{\mathbf{j}_1=(\alpha,j)} \mathcal{B}_{j_1} \left[ \prod_{k=1}^{n-2} |H_{j_k, j_{k+1}}|^2 \mathcal{B}_{j_{k+1}}^{\hat{j}_k} \right] \sum_k \frac{\Gamma_{j_{n-1}, (\beta,k)}}{\tilde{\nu}_\beta} \right) \mathcal{B}_\beta. \quad (15)$$

Next, we replace terms containing  $\mathbf{j}_{n-1}$  by their average over bath states. This replacement reads:

$$\mathcal{B}_{(\alpha_{n-1}, j_{n-1})}^{\hat{j}_{n-2}} \sum_k \frac{\Gamma_{j_{n-1}, (\beta,k)}}{\tilde{\nu}_\beta} \rightarrow \hat{\Pi}_{\alpha_{n-1}, \beta} \equiv \frac{1}{N \tilde{\nu}_\beta} \sum_{j,k} \mathcal{B}_{(\alpha_{n-1}, j_{n-1})}^{\hat{j}_{n-2}} \Gamma_{(\alpha_{n-1}, j_{n-1}), (\beta,k)}. \quad (16)$$

Here we introduce the transition matrix  $\hat{\Pi}$ . Repeating this analysis, we obtain the final expression for the propagator:

$$\mathcal{D}_{\alpha\beta} = \left( \sum_n \hat{\Pi}^n \right)_{\alpha\beta} \mathcal{B}_\beta = \left( \hat{1} - \hat{\Pi} \right)_{\alpha\beta}^{-1} \mathcal{B}_\beta. \quad (17)$$

These equations summarize the central result of this work. They connect the real-space correlation function  $\mathcal{D}$  to the level-broadening statistics  $\Gamma$ . This relation does not depend on the specific distribution of matrix elements of  $V_{\text{int}}$  or on the detailed form of the level-broadening distribution. For sufficiently large systems, the latter can be evaluated numerically using the cavity equation (8), where this approach is computationally more efficient than exact diagonalization (see, e.g., Ref. [30]). The validity of Eq. (17) reflects the applicability of the diffusion approximation to interacting disordered systems, which we test numerically in the simplest setting.

## 5 Single spin thermalisation

We consider a single-spin thermometer with level spacing  $\Delta$  coupled to the bath. The Hamiltonian reads

$$H = -\frac{\Delta}{2}\tau^z + \tau^x \otimes V + H_B. \quad (18)$$

Here  $\tau^{z,x}$  are Pauli matrices. In this case, only two types of transitions occur: from 0 to 1 and from 1 to 0. This allows the propagator to be simplified as

$$\Pi_{\alpha\beta} = (\tilde{\nu}_\alpha - \varkappa \mathcal{B}_\alpha) / \tilde{\nu}_\beta. \quad (19)$$

Using this identity, the propagator becomes

$$\hat{\mathcal{D}} = \frac{\tilde{\nu}_0 \tilde{\nu}_1 \begin{pmatrix} \mathcal{B}_0 & \frac{\mathcal{B}_1}{\tilde{\nu}_1} (\tilde{\nu}_0 - \mathcal{B}_0 \varkappa) \\ \frac{\mathcal{B}_0}{\tilde{\nu}_0} (\tilde{\nu}_1 - \mathcal{B}_1 \varkappa) & \mathcal{B}_1 \end{pmatrix}}{\varkappa (\tilde{\nu}_1 \mathcal{B}_0 + \tilde{\nu}_0 \mathcal{B}_1 - \mathcal{B}_0 \mathcal{B}_1 \varkappa)}. \quad (20)$$

We connect this propagator to the  $\tau^z$  autocorrelation function using Eq. (2). The result reads

$$\text{Tr} [\tau^z(t) \tau^z \rho] = \int \frac{d\epsilon}{2\pi} \frac{d\varkappa}{2\pi i} A(\epsilon, \varkappa) e^{\varkappa t} \frac{e^{-\beta\epsilon}}{Z}, \quad (21)$$

$$A(\epsilon, \varkappa) \equiv \begin{pmatrix} 1 \\ -1 \end{pmatrix}^T \hat{\mathcal{D}} \begin{pmatrix} 1 \\ -1 \end{pmatrix}. \quad (22)$$

Here  $Z = \int d\epsilon \nu(\epsilon) e^{-\beta\epsilon}$  denotes the partition function. We use this relation to test our theoretical prediction. We compute  $A(\epsilon, \varkappa)$  from Eq. (7) and compare it with the prediction of Eq. (20) for several models. At sufficiently long times, the correlation function is dominated by its disconnected part, i.e., by the product of two average magnetizations at the given temperature. As a result,  $A$  has a pole at  $\varkappa = 0$ . We therefore focus on models with parity symmetry, where the average spin is zero and this pole is absent, which improves precision at small frequencies.

We consider several models to verify our prediction. We start with a model in which  $H_B$  is, by construction, a random matrix, and then we consider models of interacting spins.

### 5.1 Lévy model.

In the first model,  $H_B$  is a diagonal matrix with elements drawn from a normal distribution with unit width. The matrix elements of  $V$  are i.i.d. random variables. Their signs are random, while their absolute values follow a Pareto distribution:

$$P(|v|) = \frac{g^\mu}{N} \frac{\mu}{|v|^{1+\mu}}. \quad (23)$$

Matrices with a power-law distribution of elements have been studied in Refs. [28, 31] and are known as Lévy matrices; we therefore refer to this ensemble as the Lévy model. The matrix-element scaling with  $N$  is chosen so that the level broadening remains finite in the limit  $N \rightarrow \infty$ , enabling meaningful comparisons between matrices of different sizes. We use this ensemble to test Eq. (17) in the absence of a finite second moment of interaction matrix elements. The model is further motivated by Ref. [32], where power-law matrix-element

statistics emerge during the Jacobi algorithm. We compute both  $D_{\alpha,\beta}$  and  $\mathcal{B}_\alpha$  using exact diagonalization. The corresponding numerical results are shown in Fig. 3.

Curves for the same system size diverge at low frequencies. This difference originates from interference effects, which become important on the level-spacing scale  $\delta_N \sim 1/N$ . Another finite-size effect arises from the finite number of  $\Gamma$  values used to compute the averages in Eq. (17), and it is more pronounced for heavy-tailed distributions of  $\Gamma$ . This also explains the differences between solid curves for different system sizes. As the system size increases, both sets of curves converge to the same limiting behavior.

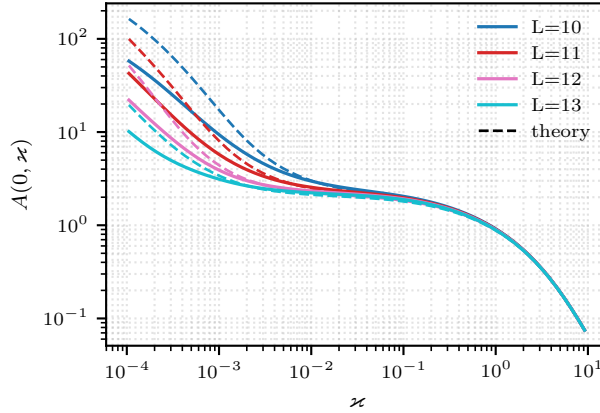


Figure 3: The Laplace transform of the  $zz$  autocorrelation function for the Lévy model is plotted for different bath sizes  $N \equiv 2^L$ . The solid lines represent the direct evaluation of Eq. (7). The dashed lines represent the theoretical evaluation of Eq. (20). We use the parameters  $\mu = 1.5$ ,  $\Delta = 0.9$ , and  $g = 0.4$ . All data are averaged over at least 30 realizations.

## 5.2 TFIM

As a second example, we consider a transverse-field Ising model (TFIM) with all-to-all interactions:

$$H_B = -\frac{1}{2} \sum_{j,k} J_{jk} \sigma_j^x \sigma_k^x + \sum_j h \sigma_j^z, \quad V = \frac{g}{\sqrt{L}} \sum_{j=1}^L \sigma_j^x. \quad (24)$$

Here, the coupling constants  $J_{jk}$  are drawn from a Gaussian distribution with width  $1/\sqrt{L}$ , where  $L$  is the number of spins in the bath and  $h = 1$ .

This model provides an example of a chaotic spin system, at least for states with energies near the center of the spectrum, where ETH is expected to hold. In contrast to the Lévy model, the number of random parameters scales only logarithmically with the Hilbert-space dimension. The interaction scaling is chosen to yield a finite scaling limit in the  $L \rightarrow \infty$  regime. The corresponding numerical results are shown in Fig. 4.

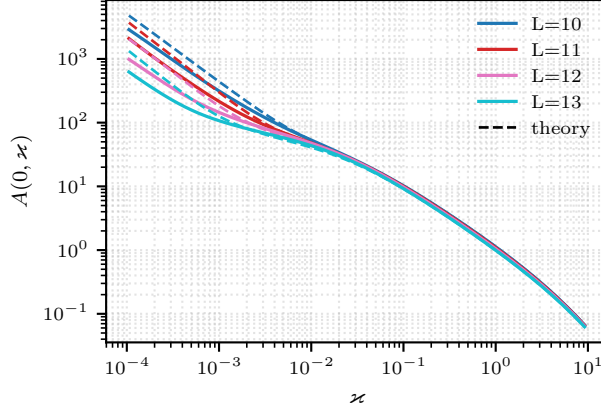


Figure 4: The Laplace transform of the  $zz$  autocorrelation function for the TFIM is plotted for different bath sizes  $L$ . The solid lines represent the direct evaluation of Eq. (7). The dashed lines represent the theoretical evaluation of Eq. (20). We use the parameters  $\Delta = 0.9$  and  $g = 0.4$ . All data are averaged over at least 30 realizations.

### 5.3 Imbrie model.

As a final example, the bath is described by the model commonly called the Imbrie model [33, 34]. The Hamiltonian of this one-dimensional model has the form

$$H_B = \sum_j \Delta_j \sigma_j^z \sigma_{j+1}^z + \sum_j (h_j \sigma_j^z + \Gamma \sigma_j^x), \quad V = g \sigma_0^x. \quad (25)$$

Here  $\Gamma = 1$ , while  $\Delta_i$  and  $h_i$  are i.i.d. random variables drawn uniformly from  $[0.8, 1.2]$  and  $[-W/2, W/2]$ , respectively. We use this model as an example of a one-dimensional interacting system with parity symmetry. The system localizes for sufficiently large disorder  $W$ . The numerical results are shown in Fig. 5 for  $W = 2$ . For larger  $W$ , the Hamiltonian eigenfunctions become more localized, which leads to poorer self-averaging of  $\hat{\Pi}$ . Equivalently, at sufficiently large disorder the spins are almost independent, so the thermometer interacts effectively only with spin 0 and the diffusive picture is no longer relevant. As a result, agreement worsens at higher  $W$ .

Overall, the agreement between the theoretical evaluation based on the diffusion picture and exact calculations is reasonable for all three models.

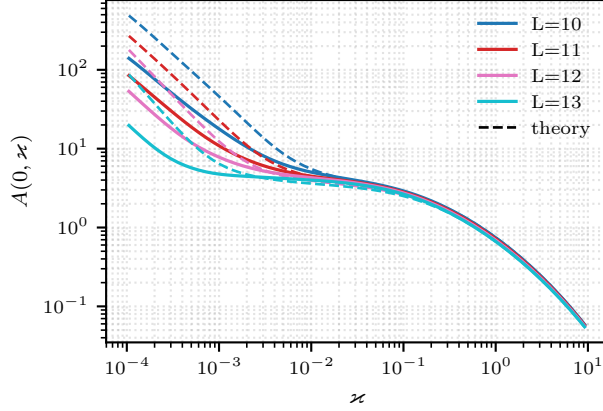


Figure 5: The Laplace transform of the  $zz$  autocorrelation function for the Imbrie model is plotted for different bath sizes  $L$ . The solid lines represent the direct evaluation of Eq. (7). The dashed lines represent the theoretical evaluation of Eq. (20). We use the parameters  $\Delta = 0.9$ ,  $g = 0.4$ , and  $W = 2$ . All data are averaged over at least 30 realizations.

## 6 Discussion and conclusion

The structure of Eq. (17) implies a conserved-probability mode. At  $z = 0$ , the matrix  $\hat{\mathbf{I}} - \hat{\mathbf{\Pi}}$  has a zero eigenvalue with right eigenvector  $\tilde{\nu}_\beta$ , which generates the zero-frequency pole of the propagator. The existence of this pole is a manifestation of probability conservation. This pole controls the long-time-limit behavior of transition probabilities:

$$p_{\alpha\beta}^{(\infty)} = \int d\epsilon \frac{\nu_\alpha(\epsilon)}{\nu(\epsilon)} s_\beta(\epsilon) \mathcal{B}_\beta(\epsilon, z=0) P(\epsilon), \quad (26)$$

where  $s_\beta$  is the left zero mode of  $\hat{\mathbf{I}} - \hat{\mathbf{\Pi}}$ , and  $\nu(\epsilon) = \sum_\alpha \nu_\alpha(\epsilon)$ . Let us introduce the bath density of states  $\nu_B(\epsilon)$ . If it is sufficiently broad, we can relate it to  $\nu_\alpha(\epsilon) = \nu_B(\epsilon - \xi_\alpha)$ . We also assume that the distribution  $P(\epsilon)$  is centered near the energy  $E$  and that its width is negligible compared to the width of  $\nu_B(\epsilon)$ . Using this notation, we can introduce the effective temperature:

$$\beta(E) \equiv \frac{d}{dE} \ln \nu_B(E), \quad (27)$$

The narrow-distribution assumption allows us to write the probabilities in the following form:

$$p_{\alpha\beta}^{(\infty)} = p_\alpha^{\text{Th}} [s_\beta \mathcal{B}_\beta]_{\epsilon=E, z=0},$$

$$p_\alpha^{\text{Th}} \equiv \frac{\nu_B(E - \xi_\alpha)}{\sum_\gamma \nu_B(E - \xi_\gamma)} = \frac{e^{-\beta(E)\xi_\alpha}}{\sum_\gamma e^{-\beta(E)\xi_\gamma}}. \quad (28)$$

This formula reflects that the system thermalises. In particular, stationary probabilities should also be thermal, i.e.,  $p_{\alpha\beta}^{(\infty)} = p_\alpha^{\text{Th}} p_\beta^{\text{Th}}$ . This implies

$$s_\beta \propto \left. \frac{\tilde{\nu}_\beta}{\mathcal{B}_\beta} \right|_{z=0}. \quad (29)$$

This relation generalizes the global-balance condition beyond Markovian kinetics. We consider the following example to illustrate it. In the self-averaging regime (e.g., Gaussian-distributed matrix elements of  $V_{\text{int}}$ ), one can define effective rates

$$\Gamma_{\alpha \rightarrow \beta} \equiv \sum_k \Gamma_{(\alpha,j),(\beta,k)}, \quad \Gamma_\alpha \equiv \sum_\beta \Gamma_{\alpha \rightarrow \beta}. \quad (30)$$

Then  $\mathcal{B}_\alpha = \tilde{\nu}_\alpha / (\varkappa + \Gamma_\alpha)$ , and the zero-mode condition gives

$$\sum_\alpha (\Gamma_{\beta \rightarrow \alpha} \tilde{\nu}_\beta - \tilde{\nu}_\alpha \Gamma_{\alpha \rightarrow \beta}) = 0, \quad (31)$$

which is the familiar global-balance equation consistent with FGR and detailed balance.

An important caveat is the regime where the typical broadening vanishes,  $\Gamma_{\text{typ}} \rightarrow 0$  as  $\varkappa \rightarrow 0$ . In that case, the stationary distribution need not be thermal. The Lévy model with  $\mu < 1$  provides a representative example [28]. This regime is closely related to MBL physics [12, 13, 8], and our results complement that literature by linking real-space relaxation to level-broadening statistics in Hilbert space.

In summary, we derived a diffusion-approximation expression for the reduced dynamics of a small thermometer coupled to a many-body bath [Eq. (17)], identified its relation to level-broadening statistics, and verified the prediction numerically in three distinct bath models (Lévy, all-to-all TFIM, and the Imbrie model; Figs. 3, 4, 5).

Several directions are natural next steps. First, extending the formalism to off-diagonal elements of the reduced density matrix would clarify dephasing in the same framework. Second, applying the approach to transport observables may help characterize slow modes in disordered interacting systems [35]. Finally, the diffusion approximation may offer practical simplifications for numerical simulations of chaotic many-body dynamics [36, 37].

## Acknowledgements

The author gratefully acknowledges K. Tikhonov and I. Gorny for insightful discussions and valuable comments on the manuscript. The author also thanks M. Feigel'man for helpful suggestions.

## References

- [1] J. M. Deutsch, *Quantum statistical mechanics in a closed system*, Physical review a **43**(4), 2046 (1991).
- [2] M. Srednicki, *Chaos and quantum thermalization*, Physical review e **50**(2), 888 (1994).
- [3] M. Srednicki, *The approach to thermal equilibrium in quantized chaotic systems*, Journal of Physics A: Mathematical and General **32**(7), 1163 (1999).
- [4] L. D'Alessio, Y. Kafri, A. Polkovnikov and M. Rigol, *From quantum chaos and eigenstate thermalization to statistical mechanics and thermodynamics*, Advances in Physics **65**(3), 239 (2016).

- [5] J. M. Deutsch, *Eigenstate thermalization hypothesis*, Reports on Progress in Physics **81**(8), 082001 (2018).
- [6] C. Schönle, D. Jansen, F. Heidrich-Meisner and L. Vidmar, *Eigenstate thermalization hypothesis through the lens of autocorrelation functions*, Physical Review B **103**(23), 235137 (2021).
- [7] J. Wang, M. H. Lamann, J. Richter, R. Steinigeweg, A. Dymarsky and J. Gemmer, *Eigenstate thermalization hypothesis and its deviations from random-matrix theory beyond the thermalization time*, Physical Review Letters **128**(18), 180601 (2022).
- [8] D. M. Basko, I. L. Aleiner and B. L. Altshuler, *Metal-insulator transition in a weakly interacting many-electron system with localized single-particle states*, Annals of physics **321**(5), 1126 (2006).
- [9] D. J. Luitz and Y. Bar Lev, *Anomalous thermalization in ergodic systems*, Physical review letters **117**(17), 170404 (2016).
- [10] M. Serbyn, Z. Papić and D. A. Abanin, *Thouless energy and multifractality across the many-body localization transition*, Physical Review B **96**(10), 104201 (2017).
- [11] P. W. Anderson *et al.*, *Absence of diffusion in certain random lattices*, Physical review **109**(5), 1492 (1958).
- [12] B. L. Altshuler, Y. Gefen, A. Kamenev and L. S. Levitov, *Quasiparticle lifetime in a finite system: A nonperturbative approach*, Physical review letters **78**(14), 2803 (1997).
- [13] I. V. Gornyi, A. D. Mirlin and D. G. Polyakov, *Interacting electrons in disordered wires: Anderson localization and low- $t$  transport*, Physical review letters **95**(20), 206603 (2005).
- [14] R. Nandkishore and D. A. Huse, *Many-body localization and thermalization in quantum statistical mechanics*, Annu. Rev. Condens. Matter Phys. **6**(1), 15 (2015).
- [15] D. A. Abanin, E. Altman, I. Bloch and M. Serbyn, *Colloquium: Many-body localization, thermalization, and entanglement*, Reviews of Modern Physics **91**(2), 021001 (2019).
- [16] K. S. Tikhonov and A. D. Mirlin, *From anderson localization on random regular graphs to many-body localization*, Annals of Physics **435**, 168525 (2021).
- [17] A. Lunkin, N. S. Ticea, S. Kumar, C. Miao, J. Choi, M. Alghadeer, I. Drozdov, D. Abanin, A. Abbas, R. Acharya *et al.*, *Evidence for a two-dimensional quantum glass state at high temperatures*, arXiv preprint arXiv:2601.01309 (2026).
- [18] D. Sherrington and S. Kirkpatrick, *Solvable model of a spin-glass*, Physical review letters **35**(26), 1792 (1975).
- [19] D. J. Thouless, P. W. Anderson and R. G. Palmer, *Solution of 'solvable model of a spin glass'*, Philosophical Magazine **35**(3), 593 (1977).
- [20] M. Mézard, G. Parisi and M. A. Virasoro, *Spin glass theory and beyond: An Introduction to the Replica Method and Its Applications*, vol. 9, World Scientific Publishing Company (1987).

- [21] A. Georges, O. Parcollet and S. Sachdev, *Quantum fluctuations of a nearly critical heisenberg spin glass*, Physical Review B **63**(13), 134406 (2001).
- [22] J. Šuntajs, J. Bonča, T. Prosen and L. Vidmar, *Quantum chaos challenges many-body localization*, Physical Review E **102**(6), 062144 (2020).
- [23] A. Morningstar, L. Colmenarez, V. Khemani, D. J. Luitz and D. A. Huse, *Avalanches and many-body resonances in many-body localized systems*, Physical Review B **105**(17), 174205 (2022).
- [24] P. Sierant and J. Zakrzewski, *Challenges to observation of many-body localization*, Physical Review B **105**(22), 224203 (2022).
- [25] K. Tikhonov and A. Mirlin, *Many-body localization transition with power-law interactions: Statistics of eigenstates*, Physical Review B **97**(21), 214205 (2018).
- [26] E. V. Doggen, F. Schindler, K. S. Tikhonov, A. D. Mirlin, T. Neupert, D. G. Polyakov and I. V. Gornyi, *Many-body localization and delocalization in large quantum chains*, arXiv preprint arXiv:1807.05051 (2018).
- [27] L. Faoro, M. V. Feigel'man and L. Ioffe, *Non-ergodic extended phase of the quantum random energy model*, Annals of Physics **409**, 167916 (2019).
- [28] P. Cizeau and J.-P. Bouchaud, *Theory of Lévy matrices*, Physical Review E **50**(3), 1810 (1994).
- [29] A. V. Lunkin and K. Tikhonov, *Local density of states correlations in the Lévy-Rosenzweig-Porter random matrix ensemble*, SciPost Physics **19**(1), 015 (2025).
- [30] K. Tikhonov and A. Mirlin, *Critical behavior at the localization transition on random regular graphs*, Physical Review B **99**(21), 214202 (2019).
- [31] E. Tarquini, G. Biroli and M. Tarzia, *Level statistics and localization transitions of lévy matrices*, Physical review letters **116**(1), 010601 (2016).
- [32] D. M. Long, P. J. Crowley, V. Khemani and A. Chandran, *Phenomenology of the prethermal many-body localized regime*, Physical Review Letters **131**(10), 106301 (2023).
- [33] G. Biroli, A. K. Hartmann and M. Tarzia, *Large-deviation analysis of rare resonances for the many-body localization transition*, Physical Review B **110**(1), 014205 (2024).
- [34] J. Z. Imbrie, *On many-body localization for quantum spin chains*, Journal of Statistical Physics **163**(5), 998 (2016).
- [35] L. Capizzi, J. Wang, X. Xu, L. Mazza and D. Poletti, *Hydrodynamics and the eigenstate thermalization hypothesis*, Physical Review X **15**(1), 011059 (2025).
- [36] R. Haghshenas, E. Chertkov, M. Mills, W. Kadow, S.-H. Lin, Y.-H. Chen, C. Cade, I. Niesen, T. Begušić, M. S. Rudolph *et al.*, *Digital quantum magnetism at the frontier of classical simulations*, arXiv preprint arXiv:2503.20870 (2025).

- [37] S. Mandrà, N. Astrakhantsev, S. Isakov, B. Villalonga, B. Ware, T. Westerhout and K. Kechedzhi, *A heuristic for matrix product state simulation of out-of-equilibrium dynamics of two-dimensional transverse-field ising models*, arXiv preprint arXiv:2511.23438 (2025).